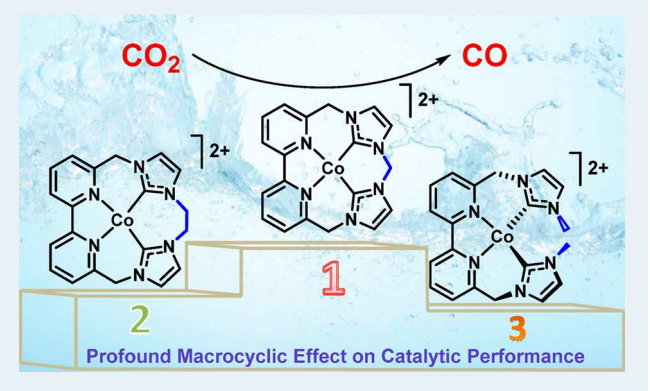


Robust and Selective Cobalt Catalysts Bearing Redox-Active Bipyridyl-N-heterocyclic Carbene Frameworks for Electrochemical CO₂ Reduction in Aqueous Solutions

Xiaojun Su,[†]
[®] Kaitlin M. McCardle,[‡]
[®] Lizhu Chen,[†]
[®] Julien A. Panetier,*,[‡]
[®] and Jonah W. Jurss*,[†]
[®]

Supporting Information

ABSTRACT: An original series of cobalt complexes bearing redox-active ligands based on bipyridyl-N-heterocyclic carbene donors has been developed for electrocatalytic CO₂ reduction in acetonitrile and aqueous solutions. The mechanism was examined by electrochemical methods and electronic structure calculations. From controlled potential electrolysis (CPE) in CH₃CN/2% H₂O solutions, **1-Co** supported by a non-macrocyclic ligand gives a Faradaic efficiency (FE) for CO₂-to-CO conversion of 78%, while **2-Co** and **3-Co** supported by tunable macrocycles afford higher selectivities for CO evolution with FEs of 91% and 98%, respectively, with the balance of charge going to H₂ production in each case. Electrochemical experiments show that the turnover frequencies across the catalyst series increase systematically from



 $66 \text{ s}^{-1} \text{ (1-Co)}$ to $570 \text{ s}^{-1} \text{ (3-Co)}$. These results demonstrate that increasing the rigidity of the ligand framework enhances catalytic activity and selectivity for CO_2 reduction over the competing H_2 evolution reaction. Indeed, catalysis was extended to water, where the same trend was observed, and CPE in CO_2 -saturated aqueous solutions using a mercury electrode revealed that 3-Co catalyzes CO_2 reduction at an overpotential of 420 mV in 0.1 M NaHCO₃ buffer with a Faradaic yield for CO of 93%. Homogeneous behavior was observed in acetonitrile solutions at carbon-based electrodes, while the catalysts were found to adsorb to mercury and exhibit heterogeneous behavior in aqueous solutions. Density functional theory (DFT) calculations and localized orbital bonding analysis indicate that the first reduction of each cobalt(II) catalyst is ligand-based to form $[Co^{II}(L^{\bullet-})]^+$ species. The second reductions are computed to transition from being ligand-localized (1-Co) to mainly metal-centered (3-Co) across the series as the ligand is more constrained, which yields a more nucleophilic cobalt center in 3-Co that enhances CO_2 reduction, kinetically and thermodynamically, with respect to 1-Co and 2-Co.

KEYWORDS: cobalt catalysts, bipyridyl-N-heterocyclic carbene, redox-active ligands, electrocatalytic CO₂ reduction, macrocycles, aqueous solution, density functional theory

INTRODUCTION

The global energy supply has long been found in chemical bonds, most notably, those of coal, oil, and natural gas. Fossil fuels are a finite resource, the combustion of which releases carbon dioxide and other airborne pollutants. The ongoing accumulation of atmospheric CO₂ has been linked to climate change and ocean acidification, among other environmental concerns, spurring the pursuit of alternative energy sources that are sustainable and carbon neutral. To achieve this goal, solar energy or renewable electricity can be used to drive the catalytic conversion of CO₂ and H₂O into energy-rich fuels (or fuel precursors) with unlimited storage capacity and compatibility with existing infrastructure. In this approach, H₂O oxidation at an anode supplies the protons and electrons that are needed at the cathode for CO₂ conversion into reduced carbon products.

However, carbon dioxide is relatively inert and its direct one-electron reduction to the highly energetic radical $CO_2^{\bullet-}$ anion requires large energy inputs to overcome activation barriers for electron transfer.⁴ Catalysts are needed to mediate the reduction of CO_2 by providing lower-energy, multielectron pathways. Importantly, reaction thermodynamics shift progressively to more positive potentials as the number of electrons and protons involved increases.⁴ As a result, proton sources are frequently added to promote the proton-coupled reduction of CO_2 . In the presence of a proton source, catalysts must be selective for CO_2 reduction (e.g., $CO_2 + 2H^+ + 2e^- \rightarrow CO + H_2O$) over the competing hydrogen evolution reaction (i.e., $2H^+ + 2e^- \rightarrow H_2$), which is comparable in energy

Received: May 3, 2019 Revised: June 19, 2019 Published: June 24, 2019



[†]Department of Chemistry and Biochemistry, University of Mississippi, University, Mississippi 38677, United States

[‡]Department of Chemistry, State University of New York at Binghamton, Binghamton, New York 13902, United States

thermodynamically and often less demanding kinetically.⁴ For large-scale fuel production, water is the ultimate reductant and thus the ideal proton source, *indeed the ideal reaction medium*, to target for sustainable CO₂ reduction catalysis.³

Existing catalysts often exhibit low turnover numbers, high overpotentials, and poor selectivity in the presence of water. Moreover, the majority of homogeneous molecular catalysts for CO₂ reduction are limited to nonaqueous solutions, including recently reported Co macrocycles. Notable exceptions include a tetranuclear iron carbonyl cluster reported by Berben and co-workers that is selective for CO₂ conversion to formate at pH 7; systems employing precious metals ruthenium, rhenium, and iridium; and several catalysts supported by tetraazamacrocycles. However, predictive design principles that would facilitate the development of better catalysts are often missing.

In this context, we recently reported a family of nickel catalysts bearing tunable tetradentate ligands comprised of a redox-active 2,2'-bipyridyl moiety and electron-rich Nheterocyclic carbene (NHC) donors, which were investigated for CO₂ reduction in CH₃CN solutions containing 2% (v/v) H₂O. 15,16 Electrochemical measurements and density functional theory (DFT) calculations showed that selectivity for CO₂ reduction versus proton reduction to H₂ depends heavily on the electronic structure of the reduced catalysts. Ligandlocalized reductions were beneficial for CO production, while metal-centered reductions allowed the formation of metalhydrides that favored H₂ evolution. 15 These results led us to explore further the synergy between the metal center and redox-active macrocycle by metal ion substitution. Observations with tetraazamacrocycles demonstrate that reactivity can be altered and varied products and/or product distributions can be accessed with different metal active sites; however, differences in reactivity as a function of metal are poorly understood, hindering predictive catalyst design. Herein, we describe a new series of catalysts based on cobalt (Scheme 1) and their electrocatalytic activity for CO₂ reduction in acetonitrile and aqueous solutions.

Scheme 1. A Series of Cobalt(II) Catalysts (1-Co, 2-Co, and 3-Co) Supported by Tunable, Redox-Active Bipyridyl-NHC Ligands

RESULTS AND DISCUSSION

Synthesis and Characterization. Cobalt complexes were synthesized by first reacting the previously reported imidazolium hexafluorophosphate ligand precursors¹⁵ with excess Ag₂O to form the corresponding silver–NHC compounds. The latter were transmetalated with CoCl₂ and subsequently stirred with sodium hexafluorophosphate to yield cobalt(II) salts with PF₆⁻ counteranions. Related procedures were developed to prepare the triflate (OTf⁻) salts of each complex to access water-soluble Co(II) catalysts. Synthetic details are provided in the Supporting Information (SI). The

cobalt complexes are designated 1-Co, 2-Co, and 3-Co, as shown in Scheme 1, regardless of their counteranions. No difference in redox potentials or reactivity was observed between the PF₆⁻ and OTf⁻ salts in CH₃CN solutions, while the triflate salts were used exclusively in studies involving aqueous solutions due to solubility. Solution magnetic susceptibilities were determined for the triflate salts in CD₃CN using the Evans method, ¹⁷ and the $\mu_{\rm eff}$ values are consistent with one unpaired electron on cobalt (Table S1, SI). The purity and composition of each paramagnetic cobalt(II) complex was confirmed by elemental analysis.

Electrochemistry in Acetonitrile Solutions. The electrochemical properties of 1-Co, 2-Co, and 3-Co were analyzed under inert atmosphere by cyclic voltammetry in anhydrous CH₃CN containing 0.1 M Bu₄NPF₆ as the supporting electrolyte (Figure 1). All potentials in nonaqueous conditions are referenced to the ferrocenium/ferrocene couple $(Fc^{+/0})$. Scanning reductively from the initial Co(II) species, the first redox events occur beyond -1.0 V vs Fc^{+/0} and have $\Delta E_{\rm p}$ values close to the ideal 59 mV peak splitting expected for a reversible, one-electron process at 25 °C. 18 At more negative potentials, a quasireversible second reduction is observed for each complex with $\Delta E_{\rm p}$ values around 80 mV. Altering the ring size of the macrocycle has a minor effect on redox potentials when comparing values of 2-Co and 3-Co. From scan-ratedependent CVs of each complex, a linear relationship is observed in plots of cathodic peak current versus the square root of the scan rate $(\nu^{1/2})$, consistent with diffusion-controlled redox processes (Figures S1-S3, SI). Redox potentials for the cobalt series are summarized in Table 1.

CVs of the cobalt family were then carried out in CO₂saturated CH3CN solutions to investigate their ability to catalyze CO₂ reduction. The first reductions shown in Figure 1 exhibit nearly no change in going from N2- to CO2-saturated solutions. However, in the presence of CO2, a more positive second reduction is observed for each complex before a catalytic wave emerges. In comparing the second reduction under N₂ and the new precatalytic wave under CO₂, positive shifts of +125, +131, and +155 mV are observed for 1-Co, 2-Co, and 3-Co, respectively. This behavior is characteristic of CO₂ binding, where the difference in potential between N₂-and CO₂-saturated solutions reflects the ability of the reduced complex to activate CO₂. ^{19,20} Carbon dioxide binding constants (K_{CO_2}) were estimated from the shift in cathodic peak potential as a function of CO2 concentration, as detailed in the Supporting Information and summarized in Table S2. The calculated K_{CO_2} values increase from 136 M⁻¹ (1-Co) to 447 M^{-1} for 3-Co, which fall within the range of CO_2 binding constants measured for other molecular cobalt complexes.² We note that the equation used to obtain these values was derived for systems that show reversible redox couples; this ideal situation is not met with our system, and thus, the CO₂ binding constants are rough estimations and should be treated as such. Upon scanning the voltage to more negative values, catalytic waves appear with peak potentials at -2.09, -2.12, and -2.26 V vs $Fc^{+/0}$ for 1-Co, 2-Co, and 3-Co, respectively.

Next, water was added to facilitate the proton-coupled reduction of CO_2 . Significant current enhancement relative to anhydrous solutions is observed in CVs under CO_2 in the presence of water for all three cobalt catalysts. Since water can also serve as a proton source for hydrogen generation, CVs were conducted in both N_2 - and CO_2 -saturated solutions to

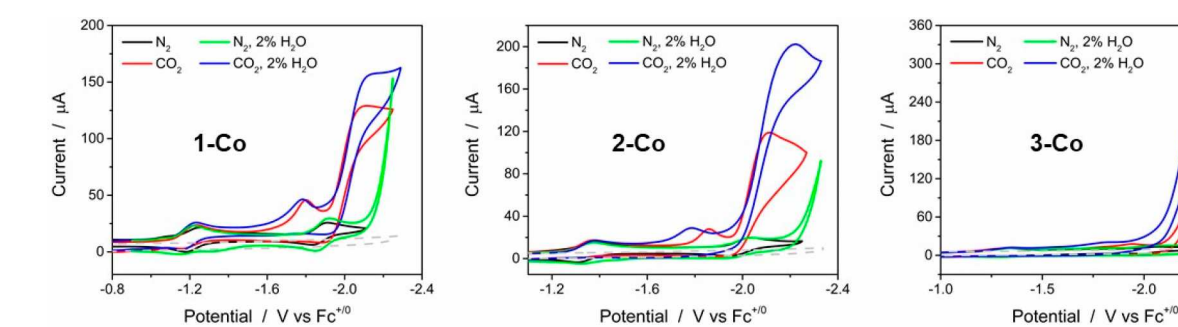


Figure 1. CVs of 1 mM 1-Co, 2-Co, and 3-Co in CH₃CN/0.1 M Bu_4NPF_6 solutions ($\nu = 100$ mV/s, glassy carbon disk) under N_2 without H_2O (black) and with 2% H₂O (green) and under CO₂ without H₂O (red) and with 2% H₂O (blue). The background under CO₂ with 2% H₂O is shown as the dashed gray curve.

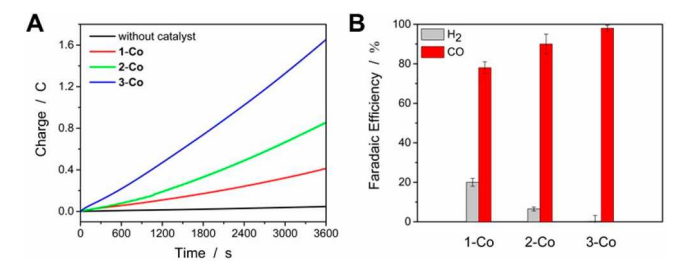
Table 1. Experimental Redox Potentials for 1-Co, 2-Co, and 3-Co from Cyclic Voltammetry in CH₃CN/0.1 M Bu₄NPF₆ Solutions

catalyst	redox potentials, E_1	redox potentials, $E_{1/2}/{ m V}^a~(\Delta E_{ m p}/{ m mV})$		
1-Co	-1.22 (63)	-1.87(75)		
2-Co	-1.34 (69)	-1.99(80)		
3-Co	-1.30 (62)	-2.03(83)		

^aRedox potentials obtained from CVs shown in Figures 1 and S1-S3

predict the selectivity for CO₂ reduction versus H⁺ reduction. CVs of 1-Co, 2-Co, and 3-Co under N₂ in the presence of H₂O display the same redox features compared to CVs under N_2 but in the absence of H_2O (Figure 1). However, at more negative potentials than the second reduction peak, all three cobalt complexes exhibit a current response indicating that proton reduction also occurs. For 1-Co, an onset potential for proton reduction is observed at E = -2.10 V, which is ~200 mV more negative than the onset potential of CO₂ reduction. In the case of 2-Co and 3-Co, the difference in onset potentials is greater and proton reduction requires more negative voltages (E = -2.20 and -2.31 V, respectively) than are necessary forCO₂ reduction, implying that the macrocyclic catalysts may possess higher selectivity for CO2 reduction under these conditions. Higher current densities were obtained when increasing the concentration of added water in CO₂-saturated CH₃CN solutions until current plateaus were reached at water concentrations exceeding 1.8%, 1.1%, and 2.0% for 1-Co, 2-Co, and 3-Co, respectively, consistent with saturation conditions (Figures S4–S6, SI).

With these results in hand, controlled potential electrolyses were carried out with each catalyst in CO₂-saturated CH₃CN solutions containing 2% H₂O to characterize the products and determine Faradaic efficiencies. Potentials were applied at E_{cat} (the potential at peak catalytic current, i_{cat}). Gaseous products in the headspace of airtight electrochemical cells were analyzed by gas chromatography after 1 h of electrolysis. The corresponding charge-time profiles are overlaid in Figure 2A. Consistent with observations from cyclic voltammetry, catalyst 1-Co displays a Faradaic efficiency of 20% for H2 and 78% for CO, whereas 2-Co exhibits higher selectivity for CO₂ reduction, generating 91% CO and 7% H₂ (Figure 2B). Remarkably, under the same conditions with 2% added H₂O, 3-Co catalyzes CO₂-to-CO conversion with a Faradaic efficiency of 98% with only trace amounts of H₂ detected. Combined Faradaic efficiencies for CO and H2 are nearly 100% across the series and strongly favor CO₂ reduction.



-2.0

Figure 2. (A) Charge versus time plots from CPEs with 0.2 mM of 1-Co, 2-Co, and 3-Co in CO₂-saturated CH₃CN/0.1 M Bu₄NPF₆ solutions containing 2% H₂O with a glassy carbon rod. (B) Faradaic efficiencies for H₂ and CO showing the product distribution of each

Control experiments were also performed to further validate these results. Controlled potential electrolyses (CPEs) of free ligand L3 and CoCl₂ salt were performed under the same conditions (Figure S7, SI). There was no increase in current above background, indicating that the cobalt complexes are responsible for the observed catalytic activity. Rinse tests were also conducted in which the glassy carbon rods were gently rinsed and subjected to the same applied potential in clean, CO₂-saturated CH₃CN/2% H₂O solutions. No catalytic current was observed, which rules out the possible formation of a heterogeneous catalyst on the electrode surface.

Standard potentials for the 2e⁻/2H⁺ reduction of CO₂-to-CO were recently reported by Matsubara for CH₃CN-H₂O mixtures covering a wide range of water concentrations, for which a reduction potential of -1.54 V vs $Fc^{+/0}$ was estimated for CH₃CN/2% H_2O (v/v).²² From this potential and $E_{cat/2}$ values, the half-wave potential of the catalytic wave²³ of each catalyst (Figure 1), overpotentials for 1-Co, 2-Co, and 3-Co are calculated to be 0.55, 0.58, and 0.72 V, respectively. Overpotentials for the nickel catalysts that are capable of CO₂ reduction under the same conditions are 0.93 and 0.92 V for 2-Ni and 3-Ni, respectively. 15

In order to probe the catalytic mechanism, the relationship of limiting catalytic current (i_{cat}) versus the concentrations of catalyst and substrate was investigated by cyclic voltammetry using electroanalytical eq 1:²⁴

$$i_{\text{cat}} = n_{\text{cat}} FA[\text{cat}] (Dk_{\text{cat}}[S]^{y})^{1/2}$$
(1)

Here, n_{cat} is the number of electrons transferred in the catalytic process (2 for CO₂ reduction to CO), F is the Faraday constant, A is the electrode surface area ($\sim 0.07 \text{ cm}^2$), [cat] is the molar concentration of the catalyst, D is its diffusion

coefficient (cm^2/s) , ¹⁸ k_{cat} is the rate constant of the catalytic reaction, and [S] is the concentration of dissolved substrates (i.e., CO₂ and acid). In CVs of 1-Co, 2-Co, and 3-Co in CO₂saturated CH₃CN/2% H₂O solutions, i_{cat} increases linearly with increasing catalyst concentration (Figures S8-S10, SI). Next, with a fixed concentration of 1 mM for each catalyst, CVs were obtained under different ratios of N₂ and CO₂ to vary the concentration of dissolved CO₂. Results from these experiments (Figures S11-S13, SI) show a linear increase in catalytic current as a function of the square root of CO₂ concentration. As previously eluded to, the concentration dependence of added H_2O was also investigated. Plots of i_{cat} as a function of [H₂O] showed a linear dependence at low concentrations with all catalysts before reaching saturation kinetics (Figures S4–S6, SI), indicating a change from secondorder to zero-order in [H₂O] for the observed catalytic rate. The combined data points to a consistent mechanism across the series that is first-order in catalyst, first-order in CO₂ (where y = 1), and second-order in proton source (where y =2) at low concentrations of water as the substrate terms are also to the one-half power in eq 1. Moreover, these results are consistent with the expected stoichiometry of the protoncoupled conversion of CO_2 to $CO + H_2O$ requiring 2 equiv of

Catalytic rates from cyclic voltammetry were first evaluated using eq 2, where i_p is the peak current observed with the catalyst in the absence of CO_2 and the quantity $(i_{cat}/i_p)^2$ is proportional to the turnover frequency (TOF).^{2.5}

TOF =
$$k_{\text{cat}}[\text{CO}_2] = \frac{Fvn_p^3}{RT} \left(\frac{0.4463}{n_{\text{cat}}}\right)^2 \left(\frac{i_{\text{cat}}}{i_p}\right)^2$$
 (2)

We note that eq 2 was derived for ideal "S-shaped" voltammograms that are characteristic of pure kinetic conditions. Sufficiently fast scan rates are often applied with this method to access a limiting catalytic current plateau. To estimate maximum TOFs, CVs as a function of scan rate were obtained in order to reach scan-rate-independent TOFs for each catalyst (Figures S14–S16, SI). From plots of TOF vs scan rate, the maximum TOFs observed for 1-Co, 2-Co, and 3-Co are 66, 186, and 570 s⁻¹, respectively, with associated $k_{\rm cat}$ values of 236, 664, and 2036 M⁻¹ s⁻¹ as the concentration of dissolved CO₂ was taken to be 0.28 M in CH₃CN. While scan-rate-independent TOFs were reached at fast scan rates, ideal steady-state behavior was not observed.

Given the nonideal behavior, Costentin and Savéant's footof-the-wave analysis (FOWA)^{25,27} was also employed via eq 3 to determine intrinsic catalytic rates:

$$\frac{i}{i_{\rm p}} = \frac{2.24\sqrt{\frac{RT}{F\nu n_{\rm p}^{3}}} 2k_{\rm cat}[{\rm CO_{2}}]}{1 + \exp\left[\frac{F}{RT}(E - E_{\rm cat/2})\right]}$$
(3)

In this electroanalytical method, competing factors such as substrate depletion and catalyst inhibition are minimized by analyzing the foot of the catalytic wave to determine the observed catalytic rate constant ($k_{\rm cat}$). From plots of $i/i_{\rm p}$ versus $1/\{1+\exp[(F/RT)(E-E_{\rm cat/2})]\}$, $k_{\rm cat}$ can be calculated from the slope of the linear portion of the curve, which gives access to the maximum TOF, where TOF = $k_{\rm cat}[{\rm CO_2}]$ under saturation conditions. Scan-rate-independent TOFs of 19, 47, and 118 s⁻¹ were determined, as shown in Figures S17–S19 (SI). Notably, comparable TOF values (within a factor of

5) are obtained between the two methods (eqs 2 and 3). In addition, the previously determined reaction orders with respect to cobalt catalyst and CO₂ were confirmed using FOWA (Figures S20–S25, SI). Estimated TOFs and product distributions from electrocatalytic studies of each complex are summarized in Table 2.

Table 2. Summary of Electrocatalysis and Product Distributions for the Cobalt Series in CH₃CN Solutions Containing 2% H₂O

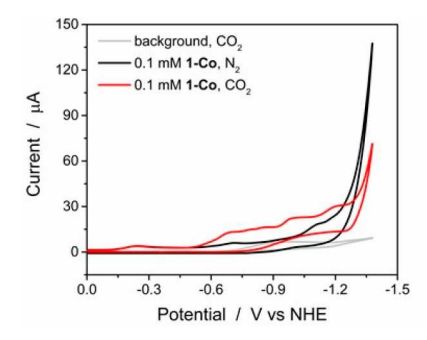
				TOF/s^{-1}	
catalyst	$E_{\rm cat}/{ m V}^a$	CO/%	$H_2/\%$	eq 2 ^b	eq 3 ^c
1-Co	-2.09	78	20	66	19
2-Co	-2.16	91	7	186	47
3-Co	-2.26	98	trace	570	118

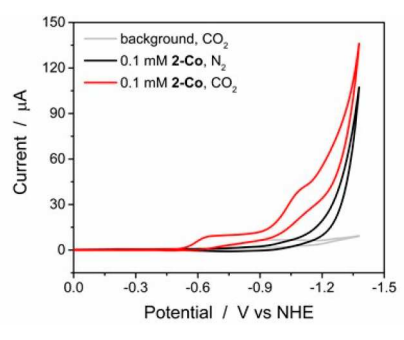
^aCatalytic peak obtained from CVs (in V versus Fc^{+/0}). ^bTOF under steady-state conditions using eq 2. ^cMaximum TOF obtained from FOWA (eq 3).

In order to compare the activity of our cobalt catalysts to known molecular catalysts, a catalytic Tafel plot was constructed (Figure S26, SI) that correlates the turnover frequency as a function of overpotential for each system. This plot allows these two properties to be assessed concurrently where the best catalysts are found toward the upper left corner. Indeed, the cobalt series compares favorably to most reported systems and significantly outperforms cobalt tetraphenylporphyrin. Page 1979.

Electrocatalytic CO₂ Reduction in Aqueous Solutions. Given the high selectivity for CO_2 reduction over proton reduction across the cobalt series in $CH_3CN/2\%$ H_2O , we sought to extend our investigation to aqueous solutions. CO_2 reduction in water is considerably more difficult, as the solubility of CO_2 drops from 0.28 M in acetonitrile to 0.033 M in water at standard conditions, while the concentration of neat H_2O is ~55 M in comparison and serves as a high-concentration proton source that can compete with CO_2 reduction to generate H_2 .

Electrocatalytic CO₂ reduction in aqueous solutions was first investigated using a glassy carbon electrode. However, no catalytic response was observed within the electrochemical window afforded by this electrode before background proton reduction occurred at the glassy carbon surface. Thus, the working electrode was switched to mercury, which is inherently more inert toward proton reduction, in order to evaluate the catalytic activity of the cobalt series in water. Initial cyclic voltammetry was performed in aqueous 0.1 M NaClO₄ under CO₂-saturation conditions (pH 4.2) and under N₂-saturation conditions using a mercury drop electrode (Figure 3). In the case of 1-Co, a significant catalytic wave assigned to proton reduction appears under N2 at roughly -1.17 V vs NHE, whereas a weaker current response is observed under CO₂. CVs of 2-Co and 3-Co exhibit similar catalytic features under N2, but with slightly more negative onset potentials at around -1.20 V vs NHE. However, prominent catalytic waves emerge in CO2-saturated solutions at -1.12 and -1.24 V for 2-Co and 3-Co, respectively, indicative of CO2 reduction and potentially higher selectivity for the macrocyclic derivatives. Notably, the maximum catalytic current observed with catalyst 3-Co is twice that of **2-Co** under CO₂ (Figure 3).





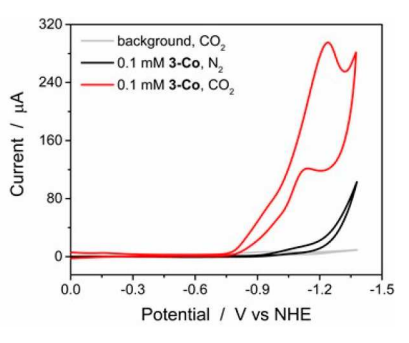


Figure 3. CVs of 0.1 mM 1-Co, 2-Co, and 3-Co in 0.1 M NaClO₄ aqueous solutions ($\nu = 100$ mV/s, mercury drop electrode) under N₂ (black) and under CO₂ (red). The background under CO₂ is shown as the gray curve.

Following cyclic voltammetry, CPEs of 1-Co, 2-Co, and 3-Co were carried out in CO₂-saturated aqueous solutions (0.1 M NaClO₄, pH 4.2) to evaluate the stability and selectivity of each catalyst under these conditions. The applied potential was varied to analyze the product distribution, as shown in Table 3.

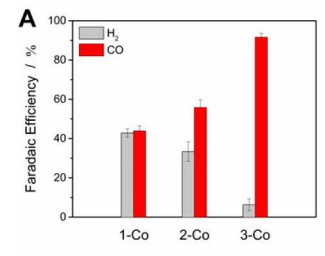
Table 3. Selectivity of Cobalt Catalysts Applied to CO₂ Reduction in CO₂-Saturated 0.1 M NaClO₄ Aqueous Solutions at Different Potentials^a

catalyst	$E_{\rm appl}/{\rm V}$ vs NHE	charge/C	$H_2/\%$	CO/%	FE/%
1-Co	-1.19	28	42	45	87
	-1.09	19	44	43	87
2-Co	-1.12	58	38	55	93
	-1.02	38	35	59	94
3-Co	-1.24	235	7	88	95
	-1.14	179	5	92	97
	-1.04	146	4	93	97

^aData obtained from 10 h of CPE for each entry (10 μ M catalyst, pH 4.2, Hg pool electrode) as detailed in the Supporting Information.

Minor changes in the ratio of $CO:H_2$ are observed, but overall, the product distributions are quite steady with differences in applied potentials of as much as 200 mV. Non-macrocyclic complex **1-Co** produces a \sim 1:1 ratio of $CO:H_2$. Across the series, selectivity increasingly favors CO_2 reduction as the 16-membered macrocycle supporting **2-Co** effects optimal Faradaic efficiencies of 59% CO and 35% H_2 , and the more rigid 15-membered macrocycle of **3-Co** enables FEs of 93% CO and 4% H_2 (Figure 4A). Furthermore, 3-fold higher charge is accumulated with **3-Co** in comparison to **2-Co**, consistent with the higher activity observed in cyclic voltammetry and the measured TOFs.

Additional studies were pursued with our champion catalyst 3-Co to determine its long-term stability in CO₂-saturated 0.1 M NaClO₄ aqueous solutions. Five consecutive 10 h electrolyses were conducted, in which the solution was resaturated with CO2 and the pH was measured after each segment before the electrolysis was resumed on the same solution (Figure 4B). The pH value of the solution changes from 4.2 to 6.0 over the course of this experiment. As shown in Table S3 (SI), a total of 724 C were passed over 50 h at an applied potential of -1.04 V vs NHE. The average charge consumed from each 10 h CPE was 145 ± 6 C with a consistent Faradaic yield of ~92% for CO evolution. Total turnovers for CO₂-to-CO conversion, specifically, are 4350 after 50 h. CVs are essentially unchanged in wave shape and catalytic current before and after electrolysis (Figure S27, SI). The catalyst also shows very little change with repeated cycles



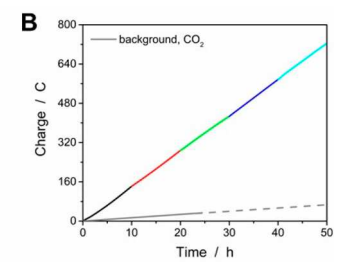


Figure 4. (A) Faradaic efficiencies of H₂ (gray) and CO (red) from CPEs with 10 μ M Co catalyst in CO₂-saturated H₂O/0.1 M NaClO₄ at a Hg pool (4 cm dia) working electrode. (B) Charge vs time plot of consecutive CPEs with 10 μ M 3-Co in CO₂-saturated aqueous 0.1 M NaClO₄. Conditions: $E_{\rm appl} = -1.04$ V vs NHE, Hg pool. CO₂ was resaturated every 10 h.

(Figure S28). We note that repeated CVs of 1-Co and 2-Co also overlay and suggest that the catalysts are stable under these conditions.

Given the gradual increase in pH of electrolyzed, CO₂saturated 0.1 M NaClO₄ solutions, electrocatalysis with 3-Co was also conducted in CO2-saturated 0.1 M NaHCO3 buffer (pH 6.7). Cyclic voltammetry shows a substantial catalytic peak under CO_2 atmosphere at E = -1.10 V vs NHE (Figure S29A, SI) with an overpotential of 420 mV (calculated from the potential at $i_{\text{cat/2}}$). CPEs were initially conducted at different applied potentials to evaluate the selectivity for CO₂ reduction over 5-h electrolyses (Table S4, SI). When holding the potential at E = -1.0 V vs NHE, the selectivity of CO₂ reduction is 93% for CO with an overall Faradaic efficiency of \sim 100% when H₂ is accounted for. As before, consecutive 10-h CPEs were carried out for a total of 40 h under these conditions in which an average charge of 117 ± 3 C was passed during each 10-h segment (Figure S29B, SI). The selectivity for CO evolution was sustained at ~93% Faradaic efficiency (Table S5, SI), and a minor change in pH was measured from 6.7 to 7.0 after 40 h. CVs taken before and after electrolysis (Figure S30, SI) indicate that 3-Co remains a durable molecular catalyst for CO₂ reduction under these conditions and operates with high activity and selectivity. In addition, control experiments were also conducted with free ligand L3 and CoCl₂ in CO₂-saturated aqueous solutions with 0.1 M NaClO₄ or 0.1 M NaHCO₃ (Figures S31 and S32, SI). As before, catalytic activity is contingent on the presence of the cobalt complexes.

Following repeated CVs or a short electrolysis, CVs of the used Hg electrode in fresh (catalyst-free) solution reveal a catalytic wave with each system, indicating that the catalyst

becomes adsorbed on the electrode surface. This behavior is analogous to the strong adsorption of nickel cyclam to mercury electrodes, which has been studied in detail. 31,32 In order to investigate whether the catalysts are molecular adsorbates or potentially decompose to an active heterogeneous catalyst, additional studies were performed with all three cobalt complexes. Following 1-h electrolyses, CVs of the used mercury electrode were obtained in fresh, catalyst-free solution showing a catalytic wave under CO₂ as shown in Figure S33 (SI). Controlled potential electrolyses were then performed in catalyst-free solution with the used mercury electrodes obtained with each catalyst. Charge-time profiles are shown in Figure S34 (SI) and the same Faradaic efficiencies for CO and H₂ evolution were measured as before (see Table 3 and Figure 4A), which strongly suggests that the catalysts are molecular adsorbates and retain their unique activities. The electrode-catalyst interactions will be the focus of future studies.

While many molecular catalysts have been reported for CO₂ reduction in organic solvents, this number is far fewer for catalysts that operate in aqueous solutions (Table S6, SI). Several cobalt-based catalysts are known to catalyze CO₂ reduction in aqueous solutions; however, they often afford poor selectivity for CO₂-to-CO conversion (<50% Faradaic yield), and long-term stability is generally absent with these catalysts. 10,12 In contrast, 3-Co generates CO with high Faradaic efficiency (>90%) over at least 40 h at an applied potential of -1.0 V vs NHE, showing a remarkable improvement in catalyst performance relative to previous molecular cobalt complexes. The steady charge accumulation and reproducible pre- and post-electrolysis CVs, in addition to the complex-dependent product distributions, strongly suggest that the catalysts are molecular in nature. Indeed, 3-Co is a remarkably stable molecular electrocatalyst for CO2 reduction with high selectivity in aqueous solutions.

Computational Results. Electronic structure calculations were performed on the cobalt(II) catalysts (denoted in this section as $[1-Co]^{2+}$, $[2-Co]^{2+}$, and $[3-Co]^{2+}$) as well as their one- and two-electron-reduced species in order to rationalize the observed reactivity and selectivity. The ω B97X-D³³ results are discussed in the main text; however, similar trends were obtained with the B3LYP-D3(BJ), 34,35 PBE0-D3(BJ), 35,36 and TPSSh³⁷ functionals (see the Supporting Information).

Experimentally, the first reductions of the Co(II) species are reversible across the series, which are followed by a quasireversible reduction in each case that gives rise to catalysis in the presence of CO₂. These reductions are of interest in understanding the difference in behavior of the cobalt complexes in catalyzing CO₂ reduction and were investigated in detail computationally.

Starting with the Co(II) species ($S = \frac{1}{2}$), our calculations indicate that the four-coordinate species are lower in energy than the five-coordinate species, in which one molecule of acetonitrile is bound to cobalt (Tables S7–S11, SI). It is worth mentioning that five-coordinate distorted square pyramidal cobalt(II) complexes have been previously isolated and characterized by X-ray crystallography and DFT calculations.³⁸ The computed structure of the four-coordinate catalyst 2 [1-Co]²⁺ (where the first superscript denotes the spin multiplicity of a given species, in this case doublet) was found to deviate from ideal square planar geometry at cobalt. For instance, the dihedral angle (τ) between the two ligand planes (CoC₂ and CoN₂) is calculated to be 24° in 2 [1-Co]²⁺, while τ is equal to

 10° and 6° in 2 [2-Co] $^{2+}$ and 2 [3-Co] $^{2+}$, respectively. This observation reflects the increased rigidity of the ligand framework in going from 1-Co to 3-Co. Localized orbital bonding analysis (LOBA) calculations indicate that the four-coordinate catalysts have one unpaired electron in the $d_{z^{2}}$ orbital (seven fully localized d-electrons, Figure S37–S39, SI), consistent with the +2 oxidation state on cobalt. This is in agreement with the solution magnetic susceptibilities measured in CD₃CN by the Evans method (Table S1, SI).

The redox potentials of the first reduction were calculated by optimizing the one-electron-reduced species in solution (acetonitrile, $\varepsilon = 35.688$). The calculated redox potentials of the cobalt complexes are in good agreement with the experimental values [Tables 1 and S12 (SI)]. Specifically, the computed reduction potentials from the four-coordinate cobalt(II) compounds to the one-electron reduced species are within 50 mV for all three complexes. In this case, all cobalt catalysts have a low-spin triplet ground state (Table S13, SI) in which one electron in the d_{z^2} orbital of the cobalt center couples ferromagnetically with one electron in the π^* orbital of the bipyridine ligand (Figure S40, SI). LOBA confirms that the cobalt center remains in the +2 oxidation state (Figures S41-S46, SI), suggesting that the first reduction is mainly ligandbased for all three cobalt catalysts. It should be noted that the open-shell singlets are calculated to be accessible, where the unpaired electron in the d₂ orbital couples antiferromagnetically with one unpaired electron in the π^* orbital of bipyridine (Table S13, SI). All DFT functionals that were tested in this study suggest that the first reduction is mainly ligand-localized (Tables S15-S17, SI) and best described as [Co^{II}(L•-)]⁺.

The second reductions were also considered computationally. The calculated potentials are again in good agreement with the experimental values [Tables 1 and S18 (SI)]. For instance, the calculated reduction potential for the non-macrocyclic catalyst is within 30 mV of the experimental value ($\Delta E = \sim 0$ mV for 2-Co and ~ 70 mV for 3-Co). In the case of the low-spin doublet 2 [1-Co] 0 , our calculations indicate that adding a second electron to the π^* orbital of the bipyridine unit is 3.6 kcal/mol lower in energy than formation of a cobalt(I) metal center (Table S19, SI). This implies that the doubly reduced species 2 [1-Co] 0 is best described as [Co $^{\rm II}({\rm L}^{2-})$] 0 [Figures 5 and S48 (SI)]. Interestingly, reduction

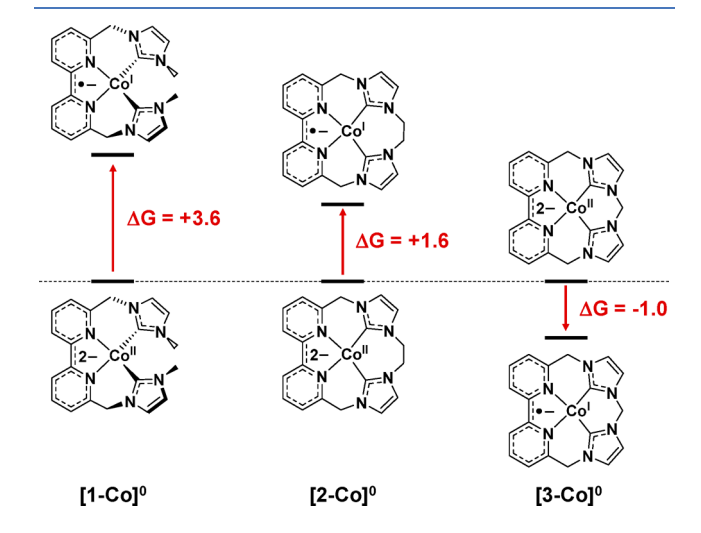


Figure 5. Summary of electronic structure calculations of the doubly reduced species and their relative energies.

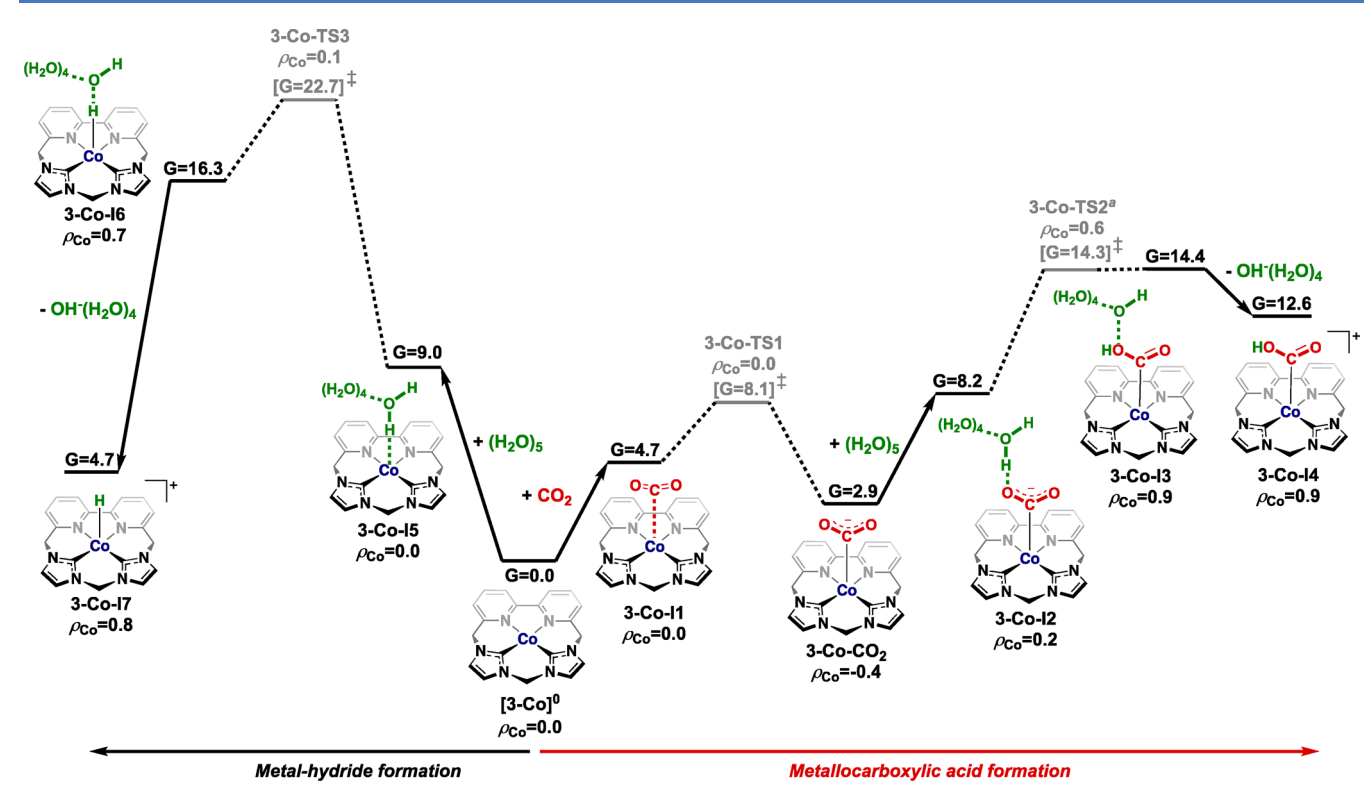


Figure 6. Computed free energy (kcal/mol) profile leading to the formation of the metallocarboxylic acid species 3-Co-I4 and metal-hydride intermediate 3-Co-I7 from the doubly reduced species $[3-Co]^0$ and CO_2 in the presence of a $(H_2O)_5$ cluster. All free energies are calculated with respect to the separated reactants. All species have a doublet ground state and the spin on cobalt is denoted as ρ_{Co} . The reverse reaction appears to be barrierless on the free-energy surface as the transition state 3-Co-TS2 has a lower zero-point energy than 3-Co-I3, offsetting the higher potential energy of the transition state with respect to the intermediate.

of the metal center becomes more accessible across the series as the ligand is more constrained in going from 1-Co to 3-Co. In the case of ${}^2[2\text{-Co}]^0$, formation of a cobalt(I) intermediate is only 1.6 kcal/mol higher in energy than reduction at the bipyridine ligand, while reduction of the metal center becomes accessible in ${}^2[3\text{-Co}]^0$ [$\Delta G = -1.0$ kcal/mol in favor of the metal reduction to yield a cobalt(I) species, Figure 5 and Table S19 (SI)]. Although the relative computed free energies are within the computational error range, our initial computational results show that for the second reduction, a more nucleophilic metal center is obtained as the ligand framework becomes more rigid. Additional test calculations using hybrid and hybrid meta-generalized gradient approximation (GGA) functionals also suggest that accessing a cobalt(I) metal center becomes more facile in going from 1-Co to 3-Co (Tables S21–23, SI).

On the basis of the experimental and computational data, we hypothesize that a more nucleophilic cobalt metal center in 3-Co is formed, which can subsequently activate and bind CO₂ more readily than in 1-Co and 2-Co. For instance, additional calculations indicate that CO₂ binding is kinetically more facile for 3-Co, with a computed free energy of activation of +8.1 kcal/mol relative to the separated reactants, compared to the other catalysts [ΔG^{\ddagger} = +12.8 kcal/mol for 1-Co and ΔG^{\ddagger} = +10.4 kcal/mol for 2-Co, Figures 6 and S35 and S36 (SI)]. Our hypothesis is further supported by the calculated CO₂ binding energies (ΔG = +6.5 kcal/mol for 1-Co, ΔG = +2.9 kcal/mol for 2-Co, and ΔG = +2.9 kcal/mol for 3-Co), which agree with the trend and experimental CO₂ binding constants measured in acetonitrile solutions [Tables S2 (SI) and Figures 6 and S35 and S36 (SI)].

In addition to CO₂ binding, we have also considered protonation of the doubly reduced species ²[Co]⁰ to give a cobalt-hydride intermediate and compared this pathway to the formation of a metallocarboxylic acid species. The computational results for 3-Co are discussed in the main text (Figure 6); however, similar trends were obtained for 1-Co and 2-Co (Figures S35 and S36, SI). In order to study the two competitive pathways computationally and locate transition states for the formation of the protonated complexes 3-Co-I4 and 3-Co-I7, explicit water molecules were incorporated into the calculations. However, the use of H₂O as the proton source leads to the formation of hydroxide anions (OH⁻), which we expect to be poorly solvated in solution (acetonitrile, $\varepsilon =$ 35.688) using the SMD approach. Previous studies have demonstrated that OH- can be stabilized by accepting three or four hydrogen bonds from water.³⁹ Therefore, calculated free energies of reactions involving proton transfer were determined by considering a (H₂O)₅ cluster, 40 which leads to a OH⁻(H₂O)₄ cluster after formation of the cobalt-hydride intermediate or metallocarboxylic acid species. We note that the formation energy of the water cluster $[5H_2O \rightarrow (H_2O)_5]$ has been ignored by referencing all computed free energies to the separated reactants: ${}^{2}[3\text{-Co}]^{0}$, CO₂, and (H₂O)₅ in a cyclic configuration. 40 Along the CO₂ reduction pathway, the metallocarboxylic acid complex 3-Co-I3 (G = 14.4 kcal/mol) is obtained by initial formation of 3-Co-I2 (G = 8.2 kcal/mol), in which the water cluster interacts with the Co-CO2 adduct (Figure 6). A transition state, 3-Co-TS2, for protonation of CO_2 was located with a modest activation barrier ($\Delta G^{\ddagger} = 6.1$ kcal/mol with respect to 3-Co-I2). The activation barrier for this last step increases to 14.3 kcal/mol with respect to 3-

 $Co]^0$, where the reactants are infinitively separated. In the transition state 3-Co-TS2, the nearby water cluster stabilizes the hydroxide anion while one proton is transferred onto CO_2 (OCO···H = 1.08 Å, Figure 7). Alternatively, the doubly

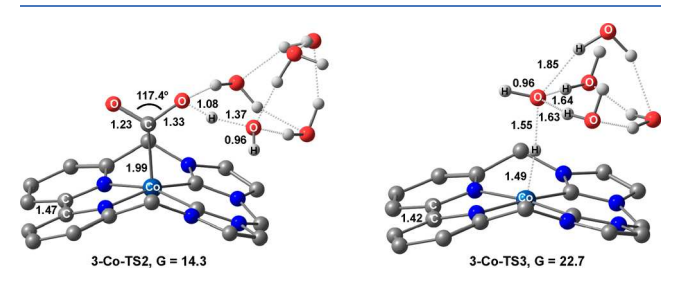


Figure 7. Computed transition states 3-Co-TS2 and 3-Co-TS3 for formation of the metallocarboxylic acid species 3-Co-I3 and cobalt—hydride complex 3-Co-I6, respectively. Computed energies are in kcal/mol, distances in angstroms, and bond angles in degrees. Nonparticipating hydrogen atoms have been omitted for clarity.

reduced complex [3-Co]⁰ can be protonated in the presence of water via initial formation of 3-Co-I5 (G = 9.0 kcal/mol). A transition state, 3-Co-TS3, was computed for the formation of a cobalt-hydride species in which a hydrogen-bonding network is used to stabilize the hydroxide anion and facilitate protonation of cobalt (Co···H = 1.49 Å, Figure 7). Overall, formation of 3-Co-I4, in which the OH⁻(H₂O)₄ cluster was removed from the calculation, is computed to be kinetically lower in energy by 8.4 kcal/mol than formation of the cobalthydride intermediate 3-Co-I7 [after removal of the OH⁻(H₂O)₄ cluster]. Similar results were observed for 1-Co and 2-Co, in which direct protonation of the doubly reduced species is kinetically less accessible ($\Delta G^{\ddagger} = 26.0 \text{ kcal/mol for}$ 1-Co-TS3 and ΔG^{\ddagger} = 23.4 kcal/mol for 2-Co-TS3) than CO₂ activation and protonation of the cobalt-CO₂ species (ΔG^{\dagger} = 12.0 kcal/mol for 1-Co-TS2 and ΔG^{\ddagger} = 13.5 kcal/mol for 2-Co-TS2). Consistent with previous reports, formation of the cobalt-hydride and/or metallocarboxylic acid intermediates are computed to be uphill in the presence of a weak Brønsted acid such as water. Here, we have considered the first protonation step, and our initial computational data indicate that CO₂ reduction is kinetically favored over proton reduction via a Co-H intermediate, which agrees with the experimental data. Notably, formation of the Co(II)-H hydride intermediate also becomes easier across the series as the metal is more nucleophilic (ΔG^{\ddagger} = +26.0 kcal/mol for 1-Co, ΔG^{\ddagger} = +23.4 kcal/mol for 2-Co, and ΔG^{\ddagger} = +22.7 kcal/mol for 3-Co). This again supports our hypothesis that a more nucleophilic metal center is formed in 3-Co. The full examination of the catalytic mechanism of all three cobalt catalysts is beyond the scope of this work and a comprehensive computational study is underway.

Comparison of Cobalt Catalysts to Nickel Analogues. The trend in selectivity for the cobalt series is similar to that of the previously reported nickel analogues. However, the cobalt complexes operate with lower overpotentials, higher activity, and greater selectivity for CO₂ reduction in the presence of H₂O compared to the nickel series, which had FEs for CO production ranging from 5 to 87% with the remaining charge balance observed as H₂ evolution.

Our electronic structure calculations indicate that the first reduction is ligand-based for each cobalt catalyst to give $[\mathsf{Co^{II}}(\mathsf{L^{\bullet -}})]^+$ species. These observations are in contrast to the

nickel series, for which electronic structure calculations found that the first reduction of the Ni(II) complexes switches from being metal-centered to ligand-based as the redox-active framework becomes increasingly rigid and planar (going from 1-Ni to 3-Ni). On this basis, by avoiding a metal-centered reduction, selectivity for CO_2 reduction was favored over the competing hydrogen evolution reaction in $CH_3CN/2\%$ H_2O solutions. Catalysts with an accessible Ni(II/I) reduction generated significantly more H_2 , presumably by facile formation of nickel—hydride intermediates, compared to 3-Ni, for which the first reduction is localized on the ligand to yield $[Ni^{II}(L^{\bullet-})]^+$.

Conversely, it is the first reduction that is ligand-localized across the cobalt catalyst series reported here. An interesting aspect of the cobalt complexes is that it is the second reduction which appears to be sensitive to structural modifications. For instance, our electronic structure calculations suggest that the non-macrocyclic complex 1-Co is at odds with its macrocyclic counterparts 2-Co and 3-Co, which each have a more accessible metal-based reduction that enhances CO2 activation and conversion, even in aqueous solutions. CO2 binding constants for the cobalt catalysts were estimated from cyclic voltammograms, whereas the CO₂ binding constants could not be reliably measured for the nickel series using the same technique. It has been shown previously with cyclam and unsaturated cylam derivatives of nickel- and cobalt-based catalysts for CO2 reduction that cobalt forms stronger bonds with CO₂ than its nickel congeners, indicative of greater charge transfer to the substrate. 21,43

A proposed mechanism is given in Figure 8 based on the experimental data. The rate law determined in acetonitrile

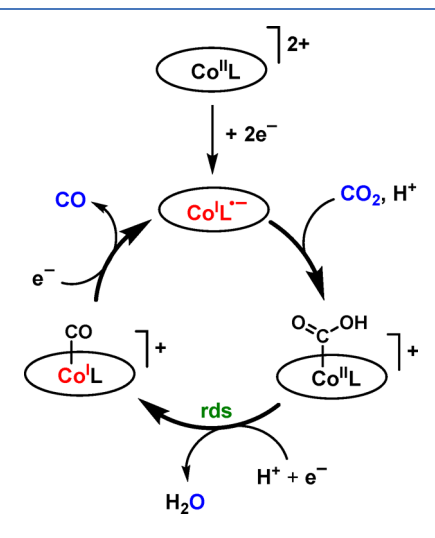


Figure 8. Proposed mechanism for electrocatalytic CO_2 reduction to CO with **3-Co** in the presence of water as a proton source. The rate-determining step (rds) at low concentrations of H_2O is indicated.

solutions with low concentrations of water as the proton source is rate = $k[\text{cat}][\text{CO}_2][\text{H}^+]^2$. Given the second-order dependence on acid concentration (at low $[\text{H}_2\text{O}]$), the second protonation event is rate-limiting under these conditions. We do not have insight into whether this step is a concerted proton-coupled reduction or a sequential process (i.e., reduction followed by protonation). This rate-determining protonation results in C–O bond cleavage and the elimination of H_2O .

While protonation of the reduced cobalt also occurs at the expense of CO_2 reduction, as no formate is observed, the more nucleophilic cobalt centers of **2-Co** and **3-Co** clearly favor CO_2 over H^+ .

CONCLUSIONS

We have presented an original series of cobalt complexes bearing 2,2'-bipyridine-linked N-heterocyclic carbenes that are active for electrocatalytic CO_2 reduction in organic and aqueous solutions using water as the proton source. The activity, selectivity, and stability of these molecular catalysts have been thoroughly investigated. From mechanistic studies, catalysis is first-order in catalyst, first-order in CO_2 , and second-order in acid (H_2O) at low concentrations, consistent with the overall reaction: $CO_2 + 2H^+ + 2e^- \rightarrow CO + H_2O$. Experimental results show that the macrocyclic effect that was previously reported for the analogous nickel catalysts also applies to the cobalt complexes reported here, as both the catalytic activity and selectivity increase with increasing rigidity of the ligand framework: 1-Co < 2-Co < 3-Co.

Our computational results indicate that after the first reduction, all complexes are best described as $[\mathrm{Co^{II}(L^{\bullet-})}]^+$ species. In the case of the second reduction, the electronic structure calculations suggest a potential effect of the macrocycle in which the reduction is switched from being ligand-based to being metal-centered across the series. On the basis of these arguments, we propose that a more nucleophilic metal center is formed in 3-Co after two reductions, which facilitates CO_2 binding with respect to 1-Co. This is consistent with the Faradaic efficiency for CO_2 -to-CO conversion of 78% in 1-Co, while 3-Co affords higher selectivities for CO evolution with a Faradaic efficiency of 98% in $\mathrm{CH}_3\mathrm{CN}/2\%$ $\mathrm{H}_2\mathrm{O}$ solutions.

These redox-active macrocycles employ NHC donors, which distinguish them from previous macrocycles for CO_2 reduction. Moreover, they are neutral ligands rather than dianionic (i.e., porphyrins and phthalocyanines) or trianionic frameworks (i.e., corroles). The overall charge of the resulting catalysts promotes water solubility with appropriately chosen counteranions. In contrast, charged functional groups, such as sulfonates and quaternary amines, must be appended to porphyrin-based systems to access water-soluble catalysts. 14

With the high selectivity afforded by the cobalt catalysts, their catalytic performance was also investigated in aqueous solutions. The trend established in CH₃CN/2% H₂O translated to aqueous solutions with relatively minor losses in selectivity. High activity and exceptional selectivity for CO₂-to-CO conversion (93%), combined with long-term stability, was found for 3-Co in both buffered and unbuffered CO₂-saturated aqueous solutions at overpotentials as low as 420 mV.

ASSOCIATED CONTENT

S Supporting Information

The Supporting Information is available free of charge on the ACS Publications website at DOI: 10.1021/acscatal.9b00708.

Experimental and computational details, synthetic procedures, characterization of cobalt complexes, electrochemical data, solution magnetic susceptibilities, tabulated results of known molecular catalysts for ${\rm CO_2}$ reduction in aqueous solutions, computational data,

localized orbital bonding analysis, Cartesians coordinates and computed energies (PDF)

AUTHOR INFORMATION

Corresponding Authors

*J.A.P. e-mail: panetier@binghamton.edu. *J.W.J. e-mail: jwjurss@olemiss.edu.

ORCID [©]

Xiaojun Su: 0000-0002-4060-0962

Kaitlin M. McCardle: 0000-0002-8464-1416

Lizhu Chen: 0000-0003-4645-6161 Julien A. Panetier: 0000-0003-4905-8396 Jonah W. Jurss: 0000-0002-2780-3415

Author Contributions

The manuscript was written through contributions of all authors. All authors have given approval to the final version of the manuscript.

Notes

The authors declare no competing financial interest.

ACKNOWLEDGMENTS

X.S., L.C., and J.W.J. thank the National Science Foundation for generous support through seed grant funding OIA-1539035 and a CAREER Award CHE-1848478. J.W.J. and J.A.P. are grateful to the University of Mississippi and SUNY Binghamton, respectively, for start-up support. This work was supported as part of the Multidisciplinary GAANN in Smart Energy Materials, a Graduate Assistance in Areas of National Need Program, funded by the U.S. Department of Education, under Award # P200A150135. DFT calculations were performed on the Spiedie cluster at Binghamton University, as well as the Extreme Science and Engineering Discovery Environment (XSEDE), which is supported by National Science Foundation grant number ACI-1548562, under allocation TG-CHE180009.

REFERENCES

- (1) (a) Feely, R. A.; Sabine, C. L.; Lee, K.; Berelson, W.; Kleypas, J.; Fabry, V. J.; Millero, F. J. Impact of anthropogenic CO₂ on the CaCO₃ system in the oceans. *Science* **2004**, *305*, *362*–366. (b) Houghton, J. Global warming. *Rep. Prog. Phys.* **2005**, *68*, 1343–1403. (c) *Climate Change 2014: Synthesis Report*; Contribution of Working Groups I, II and III to the Fifth Assessment Report of the Intergovernmental Panel on Climate Change; Core Writing Team, Pachauri, R. K., Meyer, L., Eds.; IPCC: Geneva, Switzerland, 2014. (2) Lewis. N. S.; Nocera. D. G. Powering the planet: Chemical
- (2) Lewis, N. S.; Nocera, D. G. Powering the planet: Chemical challenges in solar energy utilization. *Proc. Natl. Acad. Sci. U. S. A.* **2006**, *103*, 15729–15735.
- (3) (a) Concepcion, J. J.; Jurss, J. W.; Brennaman, M. K.; Hoertz, P. G.; Patrocinio, A. O. T.; Murakami Iha, N. Y.; Templeton, J. L.; Meyer, T. J. Making oxygen with ruthenium complexes. *Acc. Chem. Res.* 2009, 42, 1954–1965. (b) Concepcion, J. J.; House, R. L.; Papanikolas, J. M.; Meyer, T. J. Chemical approaches to artificial photosynthesis. *Proc. Natl. Acad. Sci. U. S. A.* 2012, 109, 15560–15564.
- (4) (a) Benson, E. E.; Kubiak, C. P.; Sathrum, A. J.; Smieja, J. M. Electrocatalytic and homogeneous approaches to conversion of CO₂ to liquid fuels. *Chem. Soc. Rev.* **2009**, *38*, 89–99. (b) Yui, T.; Tamaki, Y.; Sekizawa, K.; Ishitani, O. Photocatalytic reduction of CO₂: from molecules to semiconductors. *Top. Curr. Chem.* **2011**, *303*, 151–184. (c) Finn, C.; Schnittger, S.; Yellowlees, L. J.; Love, J. B. Molecular approaches to the electrochemical reduction of carbon dioxide. *Chem. Commun.* **2012**, *48*, 1392–1399. (d) Appel, A. M.; Bercaw, J. E.; Bocarsly, A. B.; Dobbek, H.; DuBois, D. L.; Dupuis, M.; Ferry, J. G.;

Fujita, E.; Hille, R.; Kenis, P. J. A.; Kerfeld, C. A.; Morris, R. H.; Peden, C. H. F.; Portis, A. R.; Ragsdale, S. W.; Rauchfuss, T. B.; Reek, J. N. H.; Seefeldt, L. C.; Thauer, R. K.; Waldrop, G. L. Frontiers, opportunities, and challenges in biochemical and chemical catalysis of CO₂ fixation. *Chem. Rev.* **2013**, *113*, 6621–6658. (e) Kang, P.; Chen, Z.; Brookhart, M.; Meyer, T. J. Electrocatalytic reduction of carbon dioxide: Let the molecules do the work. *Top. Catal.* **2015**, *58*, 30–45. (f) Takeda, H.; Cometto, C.; Ishitani, O.; Robert, M. Electrons, photons, protons, and earth-abundant metal complexes for molecular catalysis of CO₂ reduction. *ACS Catal.* **2017**, *7*, 70–88.

- (5) (a) Chapovetsky, A.; Do, T. H.; Haiges, R.; Takase, M. K.; Marinescu, S. C. Proton-assisted reduction of CO₂ by cobalt aminopyridine macrocycles. *J. Am. Chem. Soc.* **2016**, *138*, 5765–5768. (b) Ogawa, A.; Oohora, K.; Gu, W.; Hayashi, T. Electrochemical CO₂ reduction by a cobalt bipyricorrole complex: Decrease of an overpotential value derived from monoanionic ligand character of the porphyrinoid species. *Chem. Commun.* **2019**, *55*, 493–496.
- (6) Taheri, A.; Thompson, E. J.; Fettinger, J. C.; Berben, L. A. An iron electrocatalyst for selective reduction of CO₂ to formate in water: Including thermochemical insights. *ACS Catal.* **2015**, *5*, 7140–7151. (7) (a) Chen, Z.; Concepcion, J. J.; Brennaman, M. K.; Kang, P.; Norris, M. R.; Hoertz, P. G.; Meyer, T. J. Splitting CO₂ into CO and O₂ by a single catalyst. *Proc. Natl. Acad. Sci. U. S. A.* **2012**, *109*, 15606–15611. (b) Kang, P.; Chen, Z.; Nayak, A.; Zhang, S.; Meyer, T. J. Single catalyst electrocatalytic reduction of CO₂ in water to H₂+CO syngas mixtures with water oxidation to O₂. *Energy Environ. Sci.* **2014**, *7*, 4007–4012.
- (8) Nakada, A.; Ishitani, O. Selective electrocatalysis of a water-soluble rhenium(I) complex for CO₂ reduction using water as an electron donor. ACS Catal. 2018, 8, 354–363.
- (9) (a) Kang, P.; Cheng, C.; Chen, Z.; Schauer, C. K.; Meyer, T. J.; Brookhart, M. Selective electrocatalytic reduction of CO₂ to formate by water-soluble stable iridium dihydride pincer complexes. *J. Am. Chem. Soc.* **2012**, *134*, 5500–5503. (b) Kang, P.; Meyer, T. J.; Brookhart, M. Selective electrocatalytic reduction of carbon dioxide to formate by a water-soluble iridium pincer catalyst. *Chem. Sci.* **2013**, *4*, 3497–3502.
- (10) Fisher, B.; Eisenberg, R. Electrocatalytic reduction of carbon dioxide by using macrocycles of nickel and cobalt. *J. Am. Chem. Soc.* **1980**, *102*, 7361–7363.
- (11) (a) Beley, M.; Collin, J. P.; Ruppert, R.; Sauvage, J. P. Nickel(II)-cyclam: an extremely selective electrocatalyst for reduction of CO₂ in water. *J. Chem. Soc., Chem. Commun.* 1984, 1315–1316. (b) Beley, M.; Collin, J. P.; Ruppert, R.; Sauvage, J. P. Electrocatalytic reduction of carbon dioxide by nickel cyclam²⁺ in water: study of the factors affecting the efficiency and the selectivity of the process. *J. Am. Chem. Soc.* 1986, 108, 7461–7467. (c) Collin, J. P.; Jouaiti, A.; Sauvage, J. P. Electrocatalytic properties of (tetraazacyclotetradecane)nickel²⁺ and Ni₂(biscyclam)⁴⁺ with respect to carbon dioxide and water reduction. *Inorg. Chem.* 1988, 27, 1986–1990.
- (12) Tinnemans, A. H. A.; Koster, T. P. M.; Thewissen, D. H. M. W.; Mackor, A. Tetraaza-macrocyclic cobalt(II) and nickel(II) complexes as electron-transfer agents in the photo(electro)chemical and electrochemical reduction of carbon dioxide. *Recl. Trav. Chim. Pays-Bas.* 1984, 103, 288–295.
- (13) Schneider, J.; Jia, H.; Kobiro, K.; Cabelli, D. E.; Muckerman, J. T.; Fujita, E. Nickel(II) macrocycles: highly efficient electrocatalysts for the selective reduction of CO₂ to CO. *Energy Environ. Sci.* **2012**, *5*, 9502–9510.
- (14) Costentin, C.; Robert, M.; Savéant, J. M.; Tatin, A. Efficient and selective molecular catalyst for the CO₂-to-CO electrochemical conversion in water. *Proc. Natl. Acad. Sci. U. S. A.* **2015**, *112*, 6882–6886.
- (15) Su, X.; McCardle, K. M.; Panetier, J. A.; Jurss, J. W. Electrocatalytic CO₂ reduction with nickel complexes supported by tunable bipyridyl-*N*-heterocyclic carbene donors: Understanding redox-active macrocycles. *Chem. Commun.* **2018**, *54*, 3351–3354.

(16) Shirley, H.; Su, X.; Sanjanwala, H.; Talukdar, K.; Jurss, J. W.; Delcamp, J. H. Durable solar powered systems with Ni-catalysts for conversion of CO₂ or CO to CH₄. *J. Am. Chem. Soc.* **2019**, *141*, 6617–6622.

- (17) (a) Evans, D. F. The determination of the paramagnetic susceptibility of substances in solution by nuclear magnetic resonance. *J. Chem. Soc.* **1959**, 2003–2005. (b) Bain, G. A.; Berry, J. F. Diamagnetic corrections and Pascal's constants. *J. Chem. Educ.* **2008**, 85, 532–536.
- (18) Bard, A. J.; Faulkner, L. R. Electrochemical Methods: Fundamentals and Applications, 2nd ed.; John Wiley and Sons: New York, 2001.
- (19) Gangi, D. A.; Durand, R. R., Jr. Binding of carbon dioxide to cobalt and nickel tetra-aza macrocycles. *J. Chem. Soc., Chem. Commun.* **1986**, 697–699.
- (20) Schmidt, M. H.; Miskelly, G. M.; Lewis, N. S. Effects of redox potential, steric configuration, solvent, and alkali metal cations on the binding of carbon dioxide to cobalt(I) and nickel(I) macrocycles. *J. Am. Chem. Soc.* **1990**, *112*, 3420–3426.
- (21) Schneider, J.; Jia, H.; Muckerman, J. T.; Fujita, E. Thermodynamics and kinetics of CO₂, CO, and H⁺ binding to the metal centre of CO₂ reduction catalysts. *Chem. Soc. Rev.* **2012**, *41*, 2036–2051.
- (22) Matsubara, Y. Standard electrode potentials for the reduction of CO₂ to CO in acetonitrile-water mixtures determined using a generalized method for proton-coupled electron transfer reactions. ACS Energy Lett. 2017, 2, 1886–1891.
- (23) Appel, A. M.; Helm, M. L. Determining the overpotential for a molecular electrocatalyst. *ACS Catal.* **2014**, *4*, 630–633.
- (24) (a) Savéant, J. M.; Vianello, E. Potential-sweep chronoamperometry theory of kinetic currents in the case of a first order chemical reaction preceding the electron-transfer process. *Electrochim. Acta* 1963, 8, 905–923. (b) Nicholson, R. S.; Shain, I. Theory of stationary electrode polarography. Single scan and cyclic methods applied to reversible, irreversible, and kinetic systems. *Anal. Chem.* 1964, 36, 706–723.
- (25) Rountree, E. S.; McCarthy, B. D.; Eisenhart, T. T.; Dempsey, J. L. Evaluation of homogeneous electrocatalysts by cyclic voltammetry. *Inorg. Chem.* **2014**, *53*, 9983–10002.
- (26) Fujita, E.; Szalda, D. J.; Creutz, C.; Sutin, N. Carbon dioxide activation: Thermodynamics of CO_2 binding and the involvement of two cobalt centers in the reduction of CO_2 by a cobalt(I) macrocycle. *J. Am. Chem. Soc.* **1988**, *110*, 4870–4871.
- (27) (a) Costentin, C.; Drouet, S.; Robert, M.; Savéant, J.-M. Turnover numbers, turnover frequencies, and overpotential in molecular catalysis of electrochemical reactions. Cyclic voltammetry and preparative-scale electrolysis. *J. Am. Chem. Soc.* **2012**, *134*, 11235–11242. (b) Costentin, C.; Robert, M.; Savéant, J.-M. Catalysis of the electrochemical reduction of carbon dioxide. *Chem. Soc. Rev.* **2013**, *42*, 2423–2436.
- (28) Costentin, C.; Savéant, J.-M. Multielectron, multistep molecular catalysis of electrochemical reactions: Benchmarking of homogeneous catalysts. *ChemElectroChem* **2014**, *1*, 1226–1236.
- (29) Hu, X.-M.; Rønne, M. H.; Pedersen, S. U.; Skrydstrup, T.; Daasbjerg, K. Enhanced catalytic activity of cobalt porphyrin in CO_2 electroreduction upon immobilization on carbon materials. *Angew. Chem., Int. Ed.* **2017**, *56*, 6468–6472.
- (30) Creutz, C.; Schwarz, H. A.; Wishart, J. F.; Fujita, E.; Sutin, N. Thermodynamics and kinetics of carbon dioxide binding to two stereoisomers of a cobalt(I) macrocycle in aqueous solution. *J. Am. Chem. Soc.* **1991**, *113*, 3361–3371.
- (31) Balazs, G. B.; Anson, F. C. The adsorption of Ni(cyclam)⁺ at mercury electrodes and its relation to the electrocatalytic reduction of CO₂. *J. Electroanal. Chem.* **1992**, 322, 325–345.
- (32) Wu, Y.; Rudshteyn, B.; Zhanaidarova, A.; Froehlich, J. D.; Ding, W.; Kubiak, C. P.; Batista, V. S. Electrode-ligand interactions dramatically enhance CO_2 conversion to CO by the [Ni(cyclam)]-(PF₆)₂ catalyst. ACS Catal. **2017**, 7, 5282–5288.

(33) Chai, J.-D.; Head-Gordon, M. Long-range corrected hybrid density functionals with damped atom-atom dispersion corrections. *Phys. Chem. Chem. Phys.* **2008**. *10*, 6615–6620.

- (34) Becke, A. D. Density-functional thermochemistry. III. The role of exact exchange. *J. Chem. Phys.* **1993**, *98*, 5648–5652.
- (35) Grimme, S.; Ehrlich, S.; Goerigk, L. Effect of the damping function in dispersion corrected density functional theory. *J. Comput. Chem.* **2011**, 32, 1456–1465.
- (36) Adamo, C.; Barone, V. Toward reliable density functional methods without adjustable parameters: The PBE0 model. *J. Chem. Phys.* **1999**, *110*, 6158–6169.
- (37) Staroverov, V. N.; Scuseria, G. E.; Tao, J.; Perdew, J. P. Comparative assessment of a new nonempirical density functional: Molecules and hydrogen-bonded complexes. *J. Chem. Phys.* **2003**, *119*, 12129–12137.
- (38) (a) Lacy, D. C.; McCrory, C. C. L.; Peters, J. C. Studies of cobalt-mediated electrocatalytic CO_2 reduction using a redox-active ligand. *Inorg. Chem.* **2014**, *53*, 4980–4988. (b) Zhang, M.; El-Roz, M.; Frei, H.; Mendoza-Cortes, J. L.; Head-Gordon, M.; Lacy, D. C.; Peters, J. C. Visible light sensitized CO_2 activation by the tetraaza $[Co^{II}N_4H(MeCN)]^{2+}$ complex investigated by FT-IR spectroscopy and DFT calculations. *J. Phys. Chem. C* **2015**, *119*, 4645–4654.
- (39) (a) Zanuttini, D.; Gervais, B. Ground and excited states of OH⁻(H₂O), clusters. J. Phys. Chem. A **2015**, 119, 8188–8201. (b) Xantheas, S. S. Theoretical study of hydroxide ion-water clusters. J. Am. Chem. Soc. 1995, 117, 10373-10380. (c) Bankura, A.; Chandra, A. Hydration structure and dynamics of a hydroxide ion in water clusters of varying size and temperature: Quantum chemical and ab initio molecular dynamics studies. Chem. Phys. 2012, 400, 154-164. (d) Pliego, J. R., Jr; Riveros, J. M. Ab initio study of the hydroxide ion water clusters: An accurate determination of the thermodynamic properties for the processes nH₂O + OH⁻ $HO^{-}(H_{2}O)_{n}$ (n = 1-4). J. Chem. Phys. **2000**, 112, 4045-4052. (e) Agmon, N.; Bakker, H. J.; Campen, R. K.; Henchman, R. H.; Pohl, P.; Roke, S.; Thämer, M.; Hassanali, A. Protons and Hydroxide Ions in Aqueous Systems. Chem. Rev. 2016, 116, 7642-7672. (f) Egan, C. K.; Paesani, F. Assessing many-body effects of water self-ions. I: OH⁻(H₂O)_n clusters. J. Chem. Theory Comput. **2018**, 14, 1982–1997. (40) (a) Shields, R. M.; Temelso, B.; Archer, K. A.; Morrell, T. E.; Shields, G. C. Accurate Predictions of Water Cluster Formation, $(H_2O)_{n=2-10}$. J. Phys. Chem. A **2010**, 114, 11725–11737. (b) Howard, J. C.; Tschumper, G. S. Benchmark Structures and Harmonic Vibrational Frequencies Near the CCSD(T) Complete Basis Set Limit for Small Water Clusters: $(H_2O)_{n=2, 3, 4, 5, 6}$. J. Chem. Theory Comput. 2015, 11, 2126-2136.
- (41) (a) Song, J.; Klein, E. L.; Neese, F.; Ye, S. The mechanism of homogeneous CO2 reduction by Ni(cyclam): Product selectivity, concerted proton-electron transfer and C-O bond cleavage. Inorg. Chem. 2014, 53, 7500-7507. (b) Vandezande, J. E.; Schaefer, H. F. CO₂ reduction pathways on MnBr(N-C)(CO)₃ electrocatalysts. Organometallics 2018, 37, 337-342. (c) Sung, J.; Li, X.; Wolf, L. M.; Meeder, J. R.; Bhuvanesh, N. S.; Grice, K. A.; Panetier, J. A.; Nippe, M. Synergistic Effects of Imidazolium-Functionalization on fac-Mn(CO)₃ Bipyridine Catalyst Platforms for Electrocatalytic Carbon Dioxide Reduction. J. Am. Chem. Soc. 2019, 141, 6569-6582. (42) (a) Wang, M.; Chen, L.; Sun, L. Recent progress in electrochemical hydrogen production with earth-abundant metal complexes as catalysts. Energy Environ. Sci. 2012, 5, 6763-6778. (b) Thoi, V. S.; Sun, Y.; Long, J. R.; Chang, C. J. Complexes of earthabundant metals for catalytic electrochemical hydrogen generation under aqueous conditions. Chem. Soc. Rev. 2013, 42, 2388-2400.
- (43) Kelly, C. A.; Mulazzani, Q. G.; Venturi, M.; Blinn, E. L.; Rodgers, M. A. J. The thermodynamics and kinetics of CO₂ and H⁺ binding to Ni(cyclam)⁺ in aqueous solution. *J. Am. Chem. Soc.* **1995**, 117, 4911–4919.